Normative Brain Entropy Across the Lifespan

Gianpaolo Del Mauro[1], Xinglin Zeng[1], Ze Wang[1]

[1]Department of Diagnostic Radiology and Nuclear Medicine, University of Maryland School of Medicine, Baltimore, Maryland, United States

Address for correspondence:

Gianpaolo Del Mauro, PhD

Department of Diagnostic Radiology & Nuclear Medicine

University of Maryland School of Medicine

670 W Baltimore St, HSF III

Baltimore 21202, MD

+1-443-563-0699

gdelmauro@som.umaryland.edu

Abstract

Brain entropy (BEN), a measure of the complexity and irregularity of neural has emerged as a promising marker for cognitive and clinical traits. However, normative lifespan trajectories of BEN remain underexplored. In this study, we investigated age-related changes in BEN across the human lifespan using Sample Entropy (SampEn). BEN was estimated from resting-state fMRI data collected from multiple Human Connectome Project cohorts (N = 2,415, ages 8–89 years), and normative growth curves were modeled using the GAMLSS framework. Results revealed a nonlinear increase in average BEN from childhood to older adulthood, with females exhibiting significantly higher BEN than males. Regional and network-level analyses confirmed similar age-related patterns.

Introduction

In the last decades, there has been growing interest in entropy as a tool to quantify the irregularity or randomness of brain activity. Brain entropy (BEN) is linked to Shannon's Information Theory, which relates the entropy of a time-series to its information capacity (1), and to the concept of brain self-organized criticality, a state where neural interactions are delicately balanced and information processing capacity is optimized (2). Several entropic measures have been developed over the recent years to estimate the complexity of the brain signal from time-series data by quantifying the predictability of single voxel signals over time (3). Measuring brain complexity by means of entropy, however, is not straightforward, as it has been argued that complexity and entropy may diverge when complexity reaches its peak (4). Despite this limitation, BEN quantification has been successfully applied in several neuroimaging studies, showing its intertwinement with intelligence (5–7), creativity (8), psychiatric and neurological disorders (9–11), substance dependence and abuse (12, 13), pain (14), dementia (15), brain morphology (16), task-related brain activity (17), and even the state of consciousness (18, 19). Taken together, these findings support the application of BEN as a tool to detect disease-related deviations from normative trajectories. However, lifespan normative trajectories for BEN are still lacking. Previous studies have explored age-related characteristics of BEN, revealing a complex picture influenced in part by the use of different entropic measures (3). For example, some studies reported that BEN increases (5, 6, 20) or reduces (21–24) with age, while others observed that BEN-Age associations depend on the timescale considered, with finer timescales showing an increase, and more coarse timescales showing a decrease in normal aging (25). In addition, these studies were limited by specific age intervals or small sample size.

In this study, we aim at investigating the changes of Sample Entropy (SampEn) over the lifespan. SampEn has been frequently adopted to estimate BEN from resting-state fMRI (rs-fMRI) time-series (26). Measuring BEN at rest could theoretically reflect the brain's overall flexibility or readiness to respond to unpredictable stimuli (7). We will use normative modeling to estimate normative growth charts of BEN across the human lifespan. Normative modeling has only recently been introduced to neuroscience (27), and enabled to develop age-related changes of brain structural and functional properties (28, 29).

Materials and methods

Datasets and Participants

To delineate the normative trajectory of BEN across the lifespan, three datasets from the Human Connectome Project (HCP) were aggregated: HCP-Development (HCP-D) (30), HCP-Young Adults (HCP-YA) (31), and HCP-Aging (HCP-A) (30).

rs-fMRI data and BEN mapping

Each dataset provided fully pre-processed rs-fMRI data, and each participant included up to four rs-fMRI runs. In this study, only the first run was used for analyses. For the HCP-YA, acquisition parameters included: repetition time (TR) = 720ms, echo time (TE) = 33ms, resolution = $2x2x2mm^3$, encoding direction = L-R, number of slices = 72, time-points = 1200 (32). For the HCP-D/A, acquisition parameters included: repetition time (TR) = 800ms, echo time (TE) = 37ms, resolution = $2x2x2mm^3$, encoding direction = A-P, number of slices = 72, number of timepoints = 488 (30).

All data were pre-processed following a common pipeline, including a spatial and a temporal pre-processing. Briefly, the goal of spatial pre-processing is to remove spatial artefacts, and

included: correction for spatial distortions, head motion, and B_0 distortions, registration to T1-weighted structural images, normalization to MNI space, global intensity normalization, and masking out non-brain voxels. The temporal pre-processing was applied to remove confounds and non-neuronal artifacts (including physiological signals) and included high-pass temporal filtering and independent component analyses (ICA)-based artifact removal (30, 33).

Since SampEn estimation is influenced by the length of the time-series (34), HCP-YA rs-fMRI data were truncated to 488 timepoints to match the timeseries length of the other datasets (14). Before BEN computation, rs-fMRI data were smoothed with a Gaussian filter with full-width-at-half-maximum (FWHM) = 2.5 mm to mitigate the residual inter-brain registration discrepancy.

BEN maps were obtained for each rsfMRI sequence with the BEN mapping toolbox (BENtbx) using the SampEn formula (26). SampEn is calculated as the logarithmic likelihood that a small section (within a window of a length *m*) of the data that "matches" other sections will still "match" the others if the section window length increases by 1. A "match" was identified when the distance between two compared time segments was smaller than the threshold *r*.

Denote a voxel of a rsfMRI time-series as $x = [x_1, x_2, \ldots x_N]$, where *N* is the number of time points. SampEn starts with forming a series of vectors, called embedded vectors, each with m consecutive points extracted from x: $u_i = [x_i, x_i + 1, \ldots x_i + m - 1]$, where $i = N - m + 1$, and *m* is a pre-defined dimension. Using a pre-specified distance threshold *r*, $B_i^m(r)$ counts the number of $u_j (j = 1, to\ N - m, and\ j \neq i)$ whose Chebyshev distances to u_j are less than *r*, so does $B_i^m + 1\ (r)$ for the dimension of *m* + 1. By averaging across all possible vectors, it is obtained:

$$B^m(r) = \frac{1}{(N-m)(N-m-1)} \sum_{i=1}^{N-m} B_i^m(r) \qquad (1)$$

$$A^m(r) = \frac{1}{(N-m)(N-m-1)} \sum_{i=1}^{N-m} B_i^m(r) \qquad (2)$$

And the SampEn is calculated as:

$$SampEn(m, r, N, x) = -\ln\left[\frac{A^m(r)}{B^m(r)}\right] \qquad (3)$$

The window length *m* is widely set to be from 2 to 3. The embedding vector matching cut-off should be selected to avoid "no matching" (when it is too small) and "all matching" (when it is too big) (35). Both parameters have been assessed in previous publications (26, 36). In this study, a window length of 3 and a cut-off threshold of 0.6 were adopted (26).

After the computation, all BEN maps were visually inspected, and images with excessive noise or incorrect computation were discarded.

Modeling normative growth curves across the lifespan

To estimate normative growth patterns for BEN in healthy individuals across cohorts, Generalized Additive Models for Location Scale and Shape (GAMLSS) were applied to the data using the gamlss package (version 5.4.22) in R 3.6.3 (37). To estimate a GAMLSS model requires identifying the optimal distribution family for the data, followed by selecting the best-fitting model parameters for the metric of interest. Metric-specific GAMLSS models were used to generate nonlinear normative growth curves and their first derivatives. Sex-stratified growth patterns were also examined.

The fit of 29 continuous distribution families was assessed using average BEN as the reference metric. Model performance was evaluated using the Bayesian Information Criterion (BIC) (38), with lower BIC values indicating superior fit. Among the distributions examined, the best

performance was consistently demonstrated by the Skew-t type 2 (ST2) distribution, which contains four parameters: location (μ), scale (σ), skewness (ν), and kurtosis (τ).

The GAMLSS framework can be expressed in the following way:

$$Y = F\ (\mu, \sigma, \nu, \tau) \qquad (4)$$

$$\mu = X_\mu\ \beta_\mu + Z_\mu\ \gamma_\mu + \sum_i s_{\mu,i}\ (x_i)$$

$$\sigma = X_\sigma\ \beta_\sigma + Z_\sigma\ \gamma_\sigma + \sum_i s_{\sigma,i}\ (x_i)$$

$$\nu = X_\nu\ \beta_\nu + Z_\nu\ \gamma_\nu + \sum_i s_{\nu,i}\ (x_i)$$

$$\tau = X_\tau\ \beta_\tau + Z_\tau\ \gamma_\tau + \sum_i s_{\tau,i}\ (x_i)$$

In this framework, the outcome variable Y follows a probability distribution F characterized by the above-mentioned four parameters. Each parameter is modeled using a separate additive predictor, which may include fixed effects (β, with design matrix X), random effects (γ, with design matrix Z), and non-parametric smoothing functions $s_i(x_i)$ applied to covariates.

In the current analysis, age, sex, and acquisition site were included as predictors for μ and σ, while only intercept terms were modeled for ν and τ. B-spline basis functions were used to model age as a smoothing term in the equations for μ and σ (39). A series of GAMLSS models were fitted, testing age as either a fixed effect or a smoothing term with degrees of freedom (df) ranging from 1 to 9. Models with and without site as a random effect were also compared to account for acquisition site variability. Model selection was based on the BIC. Estimation used a

convergence criterion of a log-likelihood change less than 0.001 across iterations, with a maximum of 500 iterations.

The optimal model for μ included age as a smoothing term with df = 3, sex as a fixed effect, and site as a random effect. For σ, the optimal model included age and sex as fixed effects and site as a random effect. For consistency, the same model was applied for network- and regional-level BEN values. Each BEN values, denoted by *y*, was modeled as:

$$y = ST2\ (\mu, \sigma, \nu, \tau) \quad (5)$$

$$\mu = s_{\mu}\ (age, df\ = 3) + \beta_{\mu}\ (sex) + Z_{\mu}\ (site) \quad (6)$$

$$\sigma = \beta_{\sigma}^{1}\ (age) + \beta_{\sigma}^{2}\ (sex) + Z_{\sigma}\ (site) \quad (7)$$

$$\nu = \beta_{\nu} \quad (8)$$

$$\tau = \beta_{\tau} \quad (9)$$

Results

The final sample included 2415 participants, with age ranging from 8 to 89 years (Table 1).

To examine the developmental and aging trajectories of the average BEN, the normative growth patterns of its mean across the lifespan were analyzed. Average BEN exhibited an increase from early life to late adulthood. In addition, females showed significantly higher BEN than males ($p < 0.0001$) (Figure 1, Panels A–B).

Site	N	Age Mean ± SD Range	Sex M/F
HCP-YA	1073	28.78 ± 3.69 22-37	492/581
HCP-D	631	14.19 ± 3.89 8-21	294/337
HCP-A	711	59.15 ± 14.92 36-89	315/396

Table 1. Sample size, Age, and Sex for the datasets aggregated in this study.

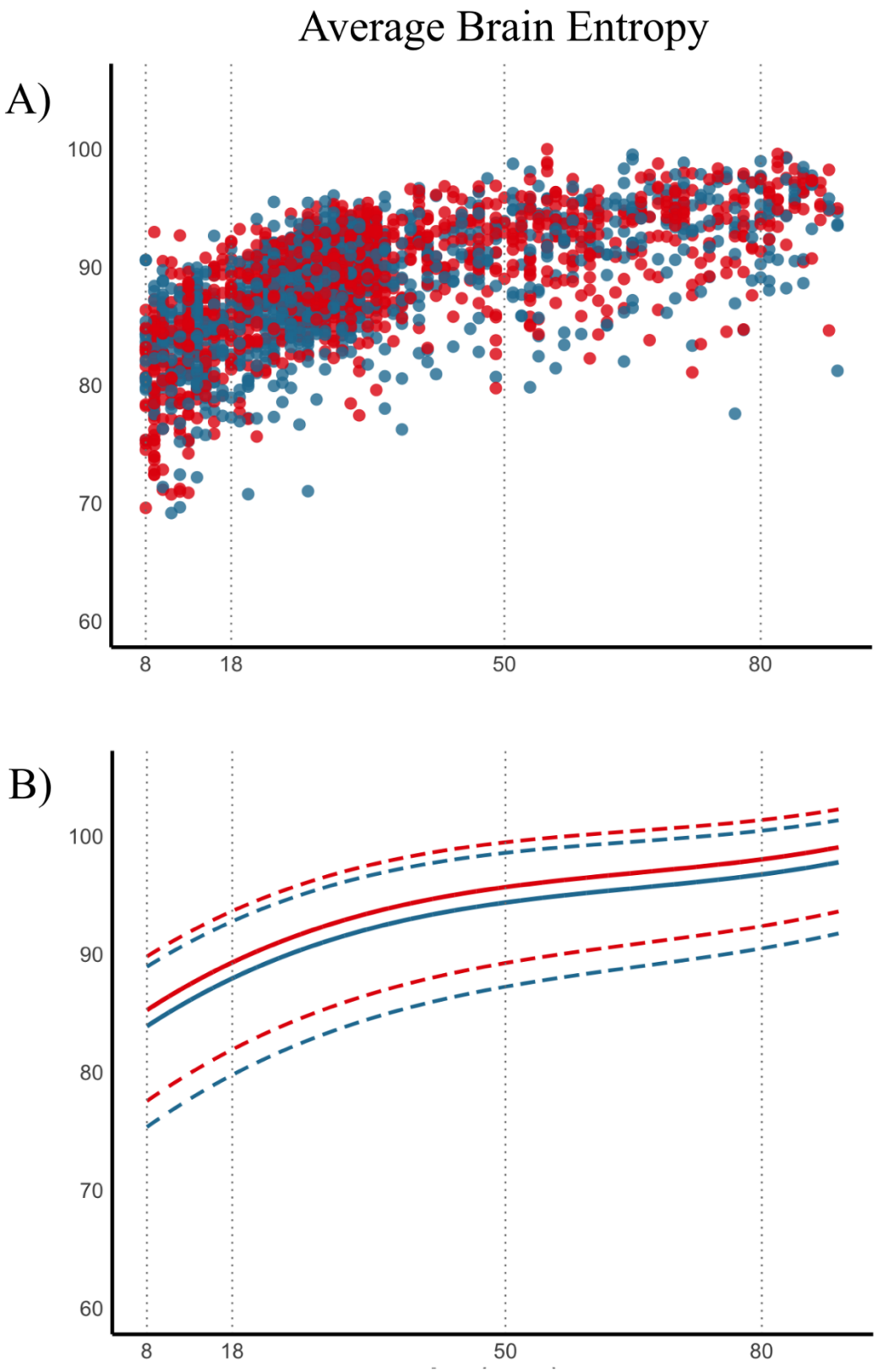

Figure 1. Normative Brain Entropy Chart. Panel A, Raw brain entropy (BEN) values across the cortex, normalized to the maximum cortical BEN. Panel B, Normative BEN Trajectories for males and females. Solid lines represent mean BEN, while dashed lines denote the 95% confidence intervals (CI).

Using the same GAMLSS model, normative growth patterns of BEN at the regional and network levels were also characterized. Brain regions were defined based on the Brainnetome atlas parcellation (40), while resting-state brain networks were defined using the Yeo seven networks atlas (41). Figure 2 shows regional maps displaying mean BEN at key lifespan benchmarks (see Figure S1 and S2 for detailed regional maps and normative trajectories). Similarly, normative BEN trajectories for resting-state networks and maps showing mean BEN values in each network at different life stages are presented in Figure 3 and 4 (see Figure S3 for detailed maps of the resting-state networks).

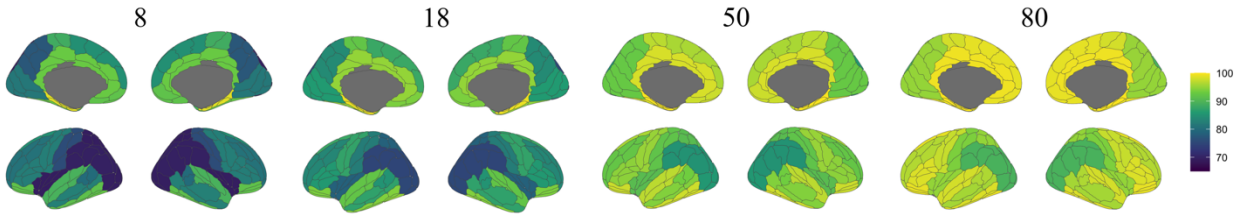

Figure 2. Regional Brain Entropy (BEN) values. Regional maps displaying local BEN values at different life stages (e.g., early childhood, adolescence, adulthood, and old age), with lighter colors representing regions with higher BEN. Brain regions were defined according to the Brainnetome atlas (40).

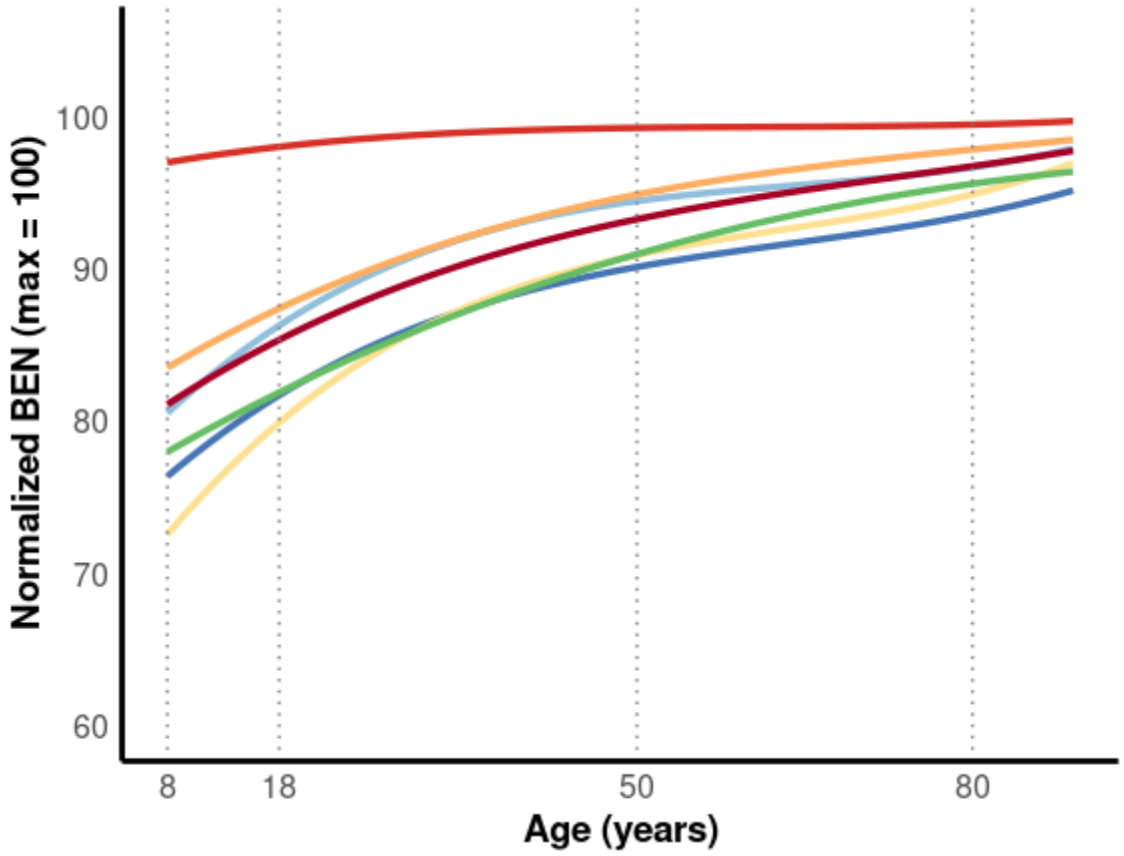

Figure 3. Normative Brain Entropy (BEN) Charts for Resting-State Brain Networks. Solid lines represent the mean BEN across different resting-state brain networks, each displayed in a different color. Networks were defined according to the Yeo seven networks atlas (41).

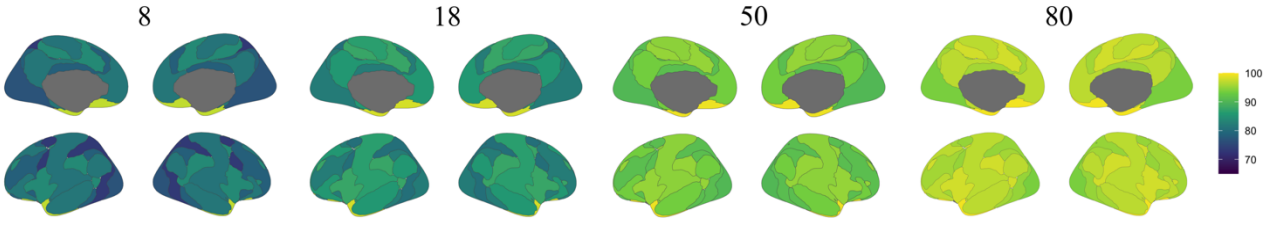

Figure 4. Brain Entropy (BEN) Across Resting-State Networks. Brain maps displaying BEN values in resting-state network at different life stages (e.g., early childhood, adolescence, adulthood, and old age), with lighter colors representing regions with higher BEN.

Discussion

This study adopted the GAMLSS framework (42) to examine the aging trajectory of BEN in an aggregated dataset with age ranging from childhood to elderhood. BEN was measured through the SampEn formula and provides an index of the randomness and irregularity of brain activity (26). Results showed an increase of BEN throughout the lifespan, with a sharper increase from childhood to young adulthood. In addition, females exhibited higher BEN than males. These results were replicated when the aging trajectory of BEN was estimated at the regional and network levels, with the exception of limbic and subcortical areas whose BEN remained stable during the lifespan, and are consistent with prior findings that focused on limited age intervals (6, 16). The increase of BEN over the lifespan suggests that brain activity becomes more irregular over time. This increase is likely to be advantageous in earlier stages of life, reflecting the brain's ability to access a higher number of states. In later stages of life, however, increased BEN might reflect a loss of structured variability and complexity of brain activity. This hypothesis is consistent with the previously reported negative correlation between BEN and fluid intelligence (6, 16).

Acknowledgements

This work was supported by the National Institute on Aging [R21AG082345, R01AG070227, R01AG081693, R21AG080518] and the University of Maryland Baltimore, Institute for Clinical & Translational Research (ICTR) [1UL1TR003098].

The authors declare no competing interests.

Bibliography

1. Shannon CE: A Mathematical Theory of Communication. *Bell System Technical Journal* 1948; 27:379–423.

2. Shew WL, Plenz D: The Functional Benefits of Criticality in the Cortex. *The Neuroscientist* 2013; 19:88–100.

3. Keshmiri S: Entropy and the Brain: An Overview. *Entropy* 2020; 22:917.

4. Lu J, Wang Z: The Systematic Bias of Entropy Calculation in the Multi-Scale Entropy Algorithm. *Entropy* 2021; 23:659.

5. Del Mauro G, Wang Z: Associations of Brain Entropy Estimated by Resting State fMRI With Physiological Indices, Body Mass Index, and Cognition. *Journal of Magnetic Resonance Imaging* 2023.

6. Wang Z: The neurocognitive correlates of brain entropy estimated by resting state fMRI. *Neuroimage* 2021; 232:117893.

7. Saxe GN, Calderone D, Morales LJ: Brain entropy and human intelligence: A resting-state fMRI study. *PLoS One* 2018; 13:e0191582.

8. Shi L, Beaty RE, Chen Q, et al.: Brain Entropy is Associated with Divergent Thinking. *Cerebral Cortex* 2019.

9. Lin C, Lee S-H, Huang C-M, et al.: Increased brain entropy of resting-state fMRI mediates the relationship between depression severity and mental health-related quality of life in late-life depressed elderly. *J Affect Disord* 2019; 250:270–277.

10. Xue S-W, Yu Q, Guo Y, Song D, Wang Z: Resting-state brain entropy in schizophrenia. *Compr Psychiatry* 2019; 89:16–21.

11. Zhou F, Zhuang Y, Gong H, Zhan J, Grossman M, Wang Z: Resting State Brain Entropy Alterations in Relapsing Remitting Multiple Sclerosis. *PLoS One* 2016; 11:e0146080.

12. Jordan T, Apostol MR, Nomi J, Petersen N: Unraveling neural complexity: Exploring brain entropy to yield mechanistic insight in neuromodulation therapies for tobacco use disorder. *Imaging Neuroscience* 2024; 2:1–17.

13. Jiang W, Cai L, Wang Z: Common hyper-entropy patterns identified in nicotine smoking, marijuana use, and alcohol use based on uni-drug dependence cohorts. *Med Biol Eng Comput* 2023.

14. Del Mauro G, Sevel LS, Boissoneault J, Wang Z: Divergent association between pain intensity and resting-state fMRI-based brain entropy in different age groups. *J Neurosci Res* 2024; 102.

15. Wang Z: Brain Entropy Mapping in Healthy Aging and Alzheimer's Disease. *Front Aging Neurosci* 2020; 12.

16. Del Mauro G, Wang Z: rsfMRI-based brain entropy is negatively correlated with gray matter volume and surface area. *Brain Struct Funct* 2025; 230:35.

17. Camargo A, Del Mauro G, Wang Z: Task-induced changes in brain entropy. *J Neurosci Res* 2024; 102.

18. Carhart-Harris RL, Leech R, Hellyer PJ, et al.: The entropic brain: a theory of conscious states informed by neuroimaging research with psychedelic drugs. *Front Hum Neurosci* 2014; 8.

19. Carhart-Harris RL: The entropic brain - revisited. *Neuropharmacology* 2018; 142:167–178.

20. Yao Y, Lu WL, Xu B, et al.: The Increase of the Functional Entropy of the Human Brain with Age. *Sci Rep* 2013; 3:2853.

21. Sokunbi MO, Cameron GG, Ahearn TS, Murray AD, Staff RT: Fuzzy approximate entropy analysis of resting state fMRI signal complexity across the adult life span. *Med Eng Phys* 2015; 37:1082–1090.

22. Dong J, Jing B, Ma X, Liu H, Mo X, Li H: Hurst Exponent Analysis of Resting-State fMRI Signal Complexity across the Adult Lifespan. *Front Neurosci* 2018; 12.

23. Niu Y, Sun J, Wang B, Yang Y, Wen X, Xiang J: Trajectories of brain entropy across lifetime estimated by resting state functional magnetic resonance imaging. *Hum Brain Mapp* 2022; 43:4359–4369.

24. Jia Y, Gu H, Luo Q: Sample entropy reveals an age-related reduction in the complexity of dynamic brain. *Sci Rep* 2017; 7:7990.

25. McIntosh AR, Vakorin V, Kovacevic N, Wang H, Diaconescu A, Protzner AB: Spatiotemporal Dependency of Age-Related Changes in Brain Signal Variability. *Cerebral Cortex* 2014; 24:1806–1817.

26. Wang Z, Li Y, Childress AR, Detre JA: Brain Entropy Mapping Using fMRI. *PLoS One* 2014; 9:e89948.

27. Rutherford S, Kia SM, Wolfers T, et al.: The Normative Modeling Framework for Computational Psychiatry. 2021.

28. Sun L, Zhao T, Liang X, et al.: Functional connectome through the human life span. 2023.

29. Bethlehem RAI, Seidlitz J, White SR, et al.: Brain charts for the human lifespan. *Nature* 2022; 604:525–533.

30. Harms MP, Somerville LH, Ances BM, et al.: Extending the Human Connectome Project across ages: Imaging protocols for the Lifespan Development and Aging projects. *Neuroimage* 2018; 183:972–984.

31. Van Essen DC, Smith SM, Barch DM, Behrens TEJ, Yacoub E, Ugurbil K: The WU-Minn Human Connectome Project: An overview. *Neuroimage* 2013; 80:62–79.

32. Smith SM, Beckmann CF, Andersson J, et al.: Resting-state fMRI in the Human Connectome Project. *Neuroimage* 2013; 80:144–168.

33. Glasser MF, Sotiropoulos SN, Wilson JA, et al.: The minimal preprocessing pipelines for the Human Connectome Project. *Neuroimage* 2013; 80:105–124.

34. Wang Z, A.M. Marcus R, Anna Rose C, John A D: Mapping brain entropy using resting state fMRI. *2013 Annual Meeting of International Society of Magnetic Resonance in Medicine 4861 (Salt Lake City, USA, 2013)* .

35. Richman JS, Moorman JR: Physiological time-series analysis using approximate entropy and sample entropy. *American Journal of Physiology-Heart and Circulatory Physiology* 2000; 278:H2039–H2049.

36. Chen X, Solomon IC, Chon KH: Comparison of the Use of Approximate Entropy and Sample Entropy: Applications to Neural Respiratory Signal. In *2005 IEEE Engineering in Medicine and Biology 27th Annual Conference*. IEEE; 2005:4212–4215.

37. Stasinopoulos DM, Rigby RA: Generalized Additive Models for Location Scale and Shape (GAMLSS) in R. *J Stat Softw* 2007; 23.

38. Neath AA, Cavanaugh JE: The Bayesian information criterion: background, derivation, and applications. *WIREs Computational Statistics* 2012; 4:199–203.

39. Di Biase MA, Tian YE, Bethlehem RAI, et al.: Mapping human brain charts cross-sectionally and longitudinally. *Proceedings of the National Academy of Sciences* 2023; 120.

40. Fan L, Li H, Zhuo J, et al.: The Human Brainnetome Atlas: A New Brain Atlas Based on Connectional Architecture. *Cerebral Cortex* 2016; 26:3508–3526.

41. Thomas Yeo BT, Krienen FM, Sepulcre J, et al.: The organization of the human cerebral cortex estimated by intrinsic functional connectivity. *J Neurophysiol* 2011; 106:1125–1165.

42. Rutherford S, Kia SM, Wolfers T, et al.: The Normative Modeling Framework for Computational Psychiatry. 2021.